Chinese Journal of Chemical Engineering 68 (2024) 224–230

Contents lists available at ScienceDirect

Chinese Journal of Chemical Engineering

journal homepage: www.elsevier.com/locate/CJChE

Full Length Article

Boron nitride silicone rubber composite foam with low dielectric and high thermal conductivity

Shuilai Qiu [1,*], Hang Wu [2], Fukai Chu [2], Lei Song [2,*]

[1] College of Safety and Ocean Engineering, China University of Petroleum-Beijing, Beijing 102249, China
[2] State Key Laboratory of Fire Science, University of Science and Technology of China, Hefei 230026, China

ARTICLE INFO

Article history:
Received 21 September 2023
Received in revised form
11 December 2023
Accepted 10 January 2024
Available online 24 February 2024

Keywords:
Foam
Composites
Dielectric properties
Thermal conductivity
Mechanical properties
Flame retardant

ABSTRACT

Silicone rubber (SR) is widely used in the field of electronic packaging because of its low dielectric properties. In this work, the porosity of the SR was improved, and the dielectric constant of the SR foam was reduced by adding expanded microspheres (EM). Then, the thermal conductivity of the system was improved by combining the modified boron nitride (f-BN). The results showed that after the f-BN was added, the dielectric constant and dielectric loss were much lower than those of pure SR. Micron-sized modified boron nitride (f-mBN) improved the dielectric and thermal conductivity of the SR foam better than that of nano-sized modified boron nitride (f-nBN), but f-nBN improved the volume resistivity, tensile strength, and thermal stability of the SR better than f-mBN. When the mass ratio of f-mBN and f-nBN is 2:1, the thermal conductivity of the SR foam reaches the maximum value of 0.808 $W \cdot m^{-1} \cdot K^{-1}$, which is 6.5 times that before the addition. The heat release rate and fire growth index are the lowest, and the improvement in flame retardancy is mainly attributed to the high thermal stability and physical barrier of f-BN.

© 2024 The Chemical Industry and Engineering Society of China, and Chemical Industry Press Co., Ltd. All rights reserved.

1. Introduction

With the rapid development and popularization of fifth-generation mobile communication technology (5G), electronic devices and equipment are developing in the direction of high frequency, high speed, high integration, and miniaturization, which puts higher requirements on the dielectric properties and thermal conductivity of 5G electronic packaging materials [1–4]. Research on the structural design of electronic packaging materials with low dielectric, high thermal conductivity, and excellent comprehensive properties is of great significance for the rapid development of 5G technology [5–7]. Additive liquid silicone rubber (ALSR) has excellent insulation, thermal stability, low dielectric, weather resistance, and processability and is widely used in the field of electronic packaging. However, it still needs to optimize its dielectric and thermal conductivity properties to further achieve the key breakthrough of 5G technology [8–10]. By adding expanded microsphere (EM) foam, the porosity of the material can be improved and the dielectric constant of the material can be reduced, but their thermal conductivity and flame retardancy of the composites were degraded due to the fact that the shell layer of EM is a flammable polymer and the interior is a flammable low-boiling-point alkane, which is not enough to satisfy the use of the electronic encapsulant for 5G [11–13]. Therefore, it is still necessary to further modify the composite material to improve its comprehensive performance and meet the actual use requirements.

At present, there are three main methods to improve the thermal conductivity of polymer matrix composites. The first is to add thermally conductive fillers to the polymer matrix, relying on the high filler content to form a thermally conductive network chain in the matrix to improve the thermal conductivity [14–16]. The second method is to use high-thermal conductivity materials to build a highly efficient thermal conductivity network inside the matrix through structural design, however, this method is relatively complicated in preparation and is not suitable for large-scale industrial production [17,18]. The third method is to use different kinds, shapes, or sizes of mixed thermally conductive fillers for compounding; for example, boron nitride (BN) layers of different sizes are used for mixed filling to achieve the purpose of improving thermal conductivity [19]. Li *et al.* [20]prepared KH550-treated BN particle-filled phenolic resin composites and investigated the effects of concentration, particle size, and hybridization of BN on the thermal conductivity of the composites. The phenolic resin filled with larger particle size BN (15 μm) showed higher thermal

* Corresponding authors.
E-mail addresses: shuilai@cup.edu.cn (S. Qiu), leisong@ustc.edu.cn (L. Song).

https://doi.org/10.1016/j.cjche.2024.01.012
1004-9541/© 2024 The Chemical Industry and Engineering Society of China, and Chemical Industry Press Co., Ltd. All rights reserved.

conductivity than that filled with smaller particle size BN (0.5 μm), which was attributed to the fact that smaller BN particles could connect the large BN particles together to form a thermally conductive pathway. Wang *et al.* [21] have studied the effect of the particle size of TiO_2 on the dielectric properties of composites, and the results show that as the size of TiO_2 decreases, the interfacial polarization within the material is enhanced and the dielectric constant (D_k) of the composite increases. Therefore, it indicates that the filling of larger-particle size thermally conductive fillers can both reduce the D_k and enhance the thermal conductivity of the material; the composite of fillers with different particle sizes can obtain higher thermal conductivity.

In this work, in order to improve the thermal conductivity and flame retardant properties of the silicone rubber (SR) composites after EM filling, the surface of BN was modified by the silane coupling agent vinyl trimethoxysilane, and the micron-sized modified BN (f-mBN) and nanometer-sized modified BN (f-nBN) were filled into the ALSR either individually or in a mixture. During the curing process, the vinyl on the surface of modified boron nitride (f-BN) can react to the Si—H bond in SR so that f-BN and the matrix are covalent bonds to form a strong interface interaction, which significantly improves the comprehensive properties of the composite foams, and to study the effects of the mixing ratio of f-BN with different particle sizes on the electrical, thermal, mechanical, and flame retardant properties of the SR composite foams.

2. Experimental

2.1. Experimental materials

Micron-sized hexagonal boron nitride (mBN) and nanosized hexagonal boron nitride (nBN) were purchased from Shanghai McLean Biochemical Technology Co., China. Two-component plus-formed liquid silicone rubber (HT-9820) was purchased from Shenzhen Hongtu Silicone Technology Co., Ltd, China. Silane coupling agent vinyl trimethoxysilane (A-171) was purchased from Huaian Heyuan Chemical Co., Ltd, China.

2.2. Preparation of f-mBN and f-nBN

Taking f-mBN as an example, the specific modification steps were as follows: a 90% aqueous ethanol solution was configured by mixing a quantitative amount of ethanol and water, and 1.0 g of A-171 was dropped into 100 ml of ethanol solution with constant stirring and mixing, and then drops of acetic acid were dropped in to adjust the pH value of the solution to about 5. 10 g of mBN was added into the above solution with ultrasonic stirring for 20 min, and then transferred to an oil bath and reacted with constant stirring at 70 °C for 4 h. The reacted solution was filtered under vacuum and washed with deionized water and ethanol for 2—3 times, and then put into a vacuum oven at 80 °C to be dried for 12 h, and the final product after drying was named f-mBN. The steps of the modification of f-nBN were the same as those described above.

2.3. Preparation of SR/EM/f-BN nanocomposites

The preparation process of SR/EM/f-BN composite foams is as follows: the weighed EM, f-mBN, and f-nBN were mixed evenly and then divided into two equal parts, respectively, added to the A component and B component of the additive molding liquid silicone rubber, and stirred thoroughly for 30 min to make the mixture homogeneous, and then the two were then mixed together with continuous stirring for 10 min, and the stirred mixture was put into the vacuum oven for defoaming treatment. The mixture will be put into the vacuum oven and vacuumed continuously at room temperature for bubble removal. After the elimination of air bubbles, according to the density of the samples under the free foaming beforehand, the corresponding mass of the mixture is slowly poured into the Polytetrafluoroethylene (PTFE) mold and then left for 5 min to eliminate a small number of air bubbles on the surface, then the mold is then sealed and put into the oven for pre-curing at 80 °C for 10 min, curing and foaming at 120 °C for 20 min, and then insulated and cured for 30 min at 100 °C. After the curing and foaming process, the samples were removed and cooled to room temperature. The nomenclature and formulations of the prepared composites are shown in Table 1.

Table 1
Raw material formulations of composite foams

Sample	SR/phr	EM/phr	f-mBN/phr	f-nBN/phr
SR	100	0	0	0
SR/EM	100	5	0	0
SR/EM/f-mBN	100	5	30	0
SR/EM/f-BN21	100	5	20	10
SR/EM/f-BN12	100	5	10	20
SR/EM/f-nBN	100	5	0	30

2.4. Characterization

Fourier transform infrared spectroscopy (FTIR) was obtained by a Nicolet 6700 spectrometer (Nicolet Instruments, USA) for qualitative analysis. X-ray diffraction (XRD) was obtained by a horizontal high-power X-ray powder diffractometer TTR-III (Rigaku Electric Co., Japan) for the physical phase analysis of the samples. Thermogravimetric analysis (TGA) was measured by the TGA Q5000 Thermogravimetric Analyzer (TA, USA) for analyzing the thermal stability of the samples under nitrogen. Scanning electron microscope (SEM) testing was carried out using a SU8220 cold field emission scanning electron microscope (Hitachi) to observe the surface morphology of the samples. The dielectric constant and dielectric loss were measured by a ZJD-C dielectric constant tester (Beijing AVIC Times Instrument Co., Ltd., China). The volume resistivity was measured and calculated by a ZC36 high resistivity meter (Shanghai Precision Instrument Co., Ltd., China). Thermal conductivity was obtained by a HOTdisk 2500s thermal constant analyzer. A cone calorimetry test was carried out on a cone calorimeter (Suzhou TESTech Testing Instrument Technology Co., Ltd., China), and the thermal radiation flux is 35 $kW \cdot m^{-2}$.

3. Results and Discussion

3.1. Structural and morphological characterization of boron nitride and modified boron nitride

For example, the structure and thermal stability of mBN and f-mBN were characterized using IR, XRD, and TGA tests. As shown in Fig. 1(a), the IR spectra of mBN showed a broad peak at 1389 cm^{-1} and a sharp peak at 815 cm^{-1}, which corresponded to the in-plane stretching vibration of B—N and the out-of-plane bending vibration of B—N—B, respectively, and the absorption peak at 3435 cm^{-1} corresponded to the stretching vibration of the surface —OH of mBN. The IR spectra of f-mBN showed an absorption peak at 1100 cm^{-1} corresponding to the stretching vibration of the Si—O binding, and a weak absorption peak at 1612 cm^{-1}, which can be attributed to the stretching vibration of the C═C double bond. Fig. 1(b) shows the XRD patterns of mBN and f-mBN. mBN has several representative diffraction peaks at 26.6°, 41.5°, 43.8°, 50.1°, and 55.1° corresponding to the (0 0 2) (1 0 0), (1 0 1), (1 0 2), and (0

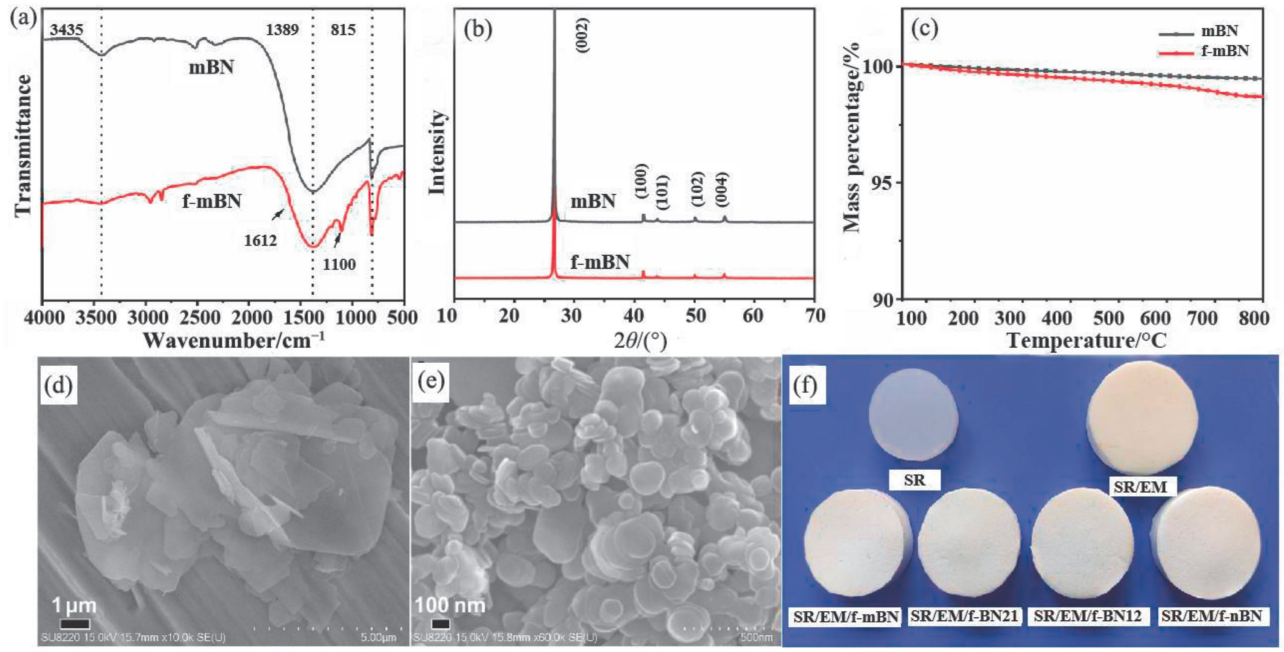

Fig. 1. (a) FT-IR spectra; (b) XRD patterns; (c) TGA curves of mBN and f-mBN; SEM images of (d) f-mBN and (e) f-nBN; (f) digital photo of SR and its composite foams.

0 4) interlayer crystal planes, respectively, and the same diffraction peaks are present for f-mBN at the corresponding angles, which indicates that f-mBN has not undergone significant changes in the crystal structure after modification. The thermal stability and structure of mBN and f-mBN were investigated by TGA curves under nitrogen, as shown in Fig. 1(c), mBN has excellent thermal stability without obvious thermal mass loss processes, and the final mass loss at 800 °C is only 0.53% (mass), which can correspond to the thermal elimination of a small amount of impurities on the surface. The mass loss of the modified f-mBN at 800 °C is 1.29% (mass), and the extra mass loss is caused by the thermal elimination of siloxane groups grafted on the surface. Fig. 1(d) and (e) show the SEM images of f-mBN and f-nBN. It can be seen that f-mBN exhibits a relatively complete irregular lamellar morphology, the mBN has a large aspect ratio, and it is easier to form a thermally conductive pathway inside the substrate. In contrast, the particle size of nBN is much smaller, with a transverse size between 100 and 500 nm, showing a circular flake-like morphology. Fig. 1(f) shows the macroscopic digital photographs of SR and its composite foams under free foaming conditions, and it can be seen that the pure SR is translucent with a smooth and flat surface. The composite foams with different sizes of f-BN added have little change in color and almost no difference in size, but their surface is rougher and has a frosted feel.

3.2. Electrical properties of SR/EM/f-BN composite foams

Fig. 2(a) and (b) show the D_k and D_f of SR and its composite foams at 1 MHz; the D_k of pure SR is 3.16, which cannot meet the requirements of 5G for electronic packaging materials. After the addition of f-BN with different particle sizes, the D_k of each composite foam has a different magnitude of decrease. As the particle size of modified BN decreases, the D_k of the composite foam increases, which is due to the fact that the smaller the particle size of BN, the larger the specific surface area, the larger the interfacial area formed with the substrate, and the interfacial polarization inside the material is enhanced, and thus the D_k rises. After adding EM and f-BN, the change of D_f in composite foams was similar to that of D_k. The D_f of pure SR was 0.00948, and the D_f of SR/EM foam was reduced to 0.00694 after the addition of five parts of EM and foaming, but the D_f of composite foam was slightly increased after the addition of f-BN, which was caused by the loss of interfacial dipole relaxation, which is similar to the change of D_k. This is because the smaller the f-BN particle size is, the stronger the interfacial polarization is inside the composites, and the resulting interfacial dipole relaxation loss is also higher, so D_f increases.

Fig. 2(c) shows the volume resistivity of SR and its composite foams. The main chain of the SR consists of repeating Si—O—Si units, which have excellent electrical insulating properties, and the figure shows that the volume resistivity of pure SR is 5.6×10^{15} Ω·cm. After the addition of f-BN with different particle sizes, the volume resistivities of the composite foams are substantially increased to 16.5×10^{15} to 22.8×10^{15} Ω·cm. It can be noticed that the volume resistivity of the composite foams increases continuously with the increase in particle size of BN, which may be due to the stronger interaction of the small-sized f-BN with the matrix and the stronger binding of the carrier movement within the matrix, so that the composites with the addition of nano-sized f-nBN have a higher volume resistivity. Fig. 2(d) shows the thermal conductivity of SR and its composite foams. Pure SR has a low thermal conductivity of 0.229 $W \cdot m^{-1} \cdot K^{-1}$ because of poor crystallinity and severe scattering of internal phonons at defects such as grain boundaries, *etc*. The comparison revealed that the thermal conductivity of the four samples with f-BN added was ranked as "SR/EM/f-nBN < SR/EM/f-mBN < SR/EM/f-BN12 < SR/EM/f-BN21". The enhancement efficiency of the thermal conductivity is greater for the f-mBN than that of the f-nBN because the larger-sized thermally conductive filler can reduce the contact area with the polymer matrix and lower the interfacial thermal resistance to increase the thermal conductivity. While the smaller-sized thermally conductive filler has a larger surface area and a larger interfacial thermal resistance, the probability of being covered by the

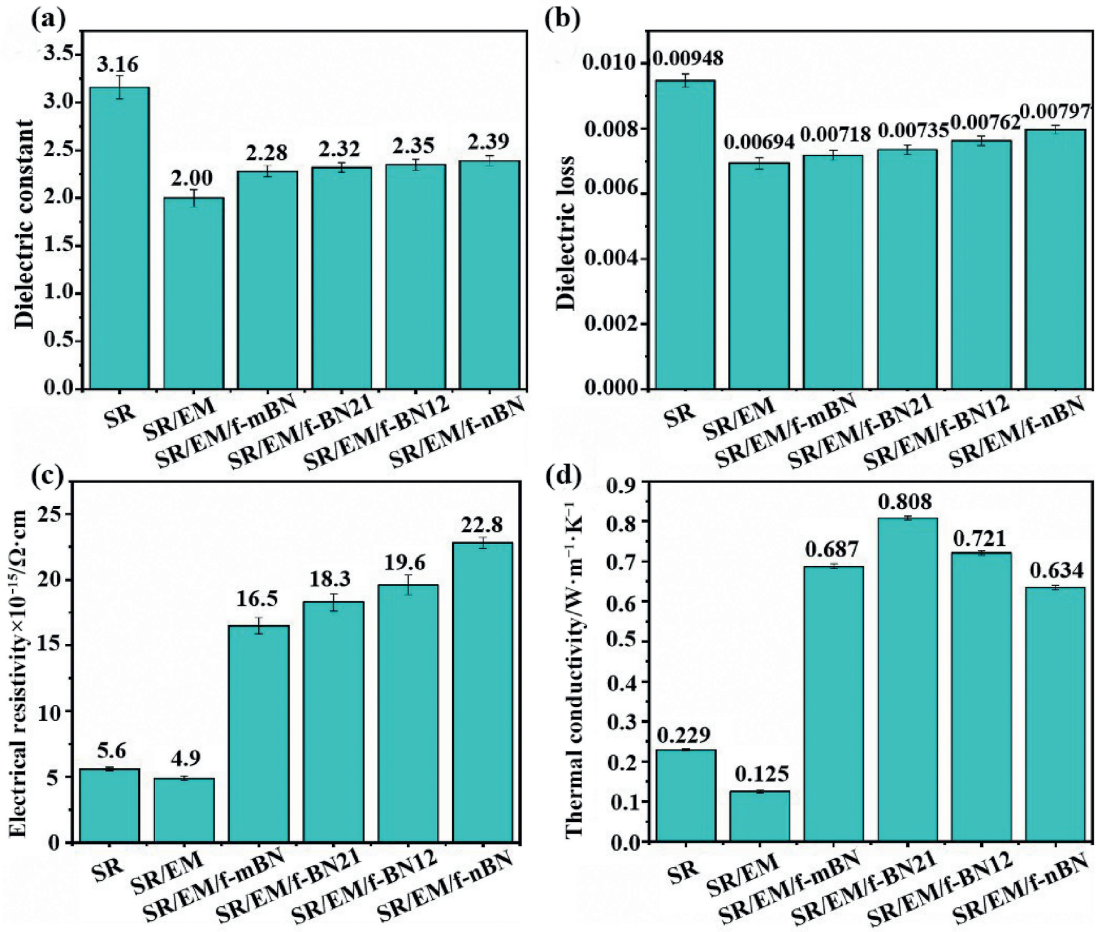

Fig. 2. (a) Dielectric constant; (b) dielectric loss; (c) electric volume resistivity; and (d) thermal conductivity of SR and its composite foams.

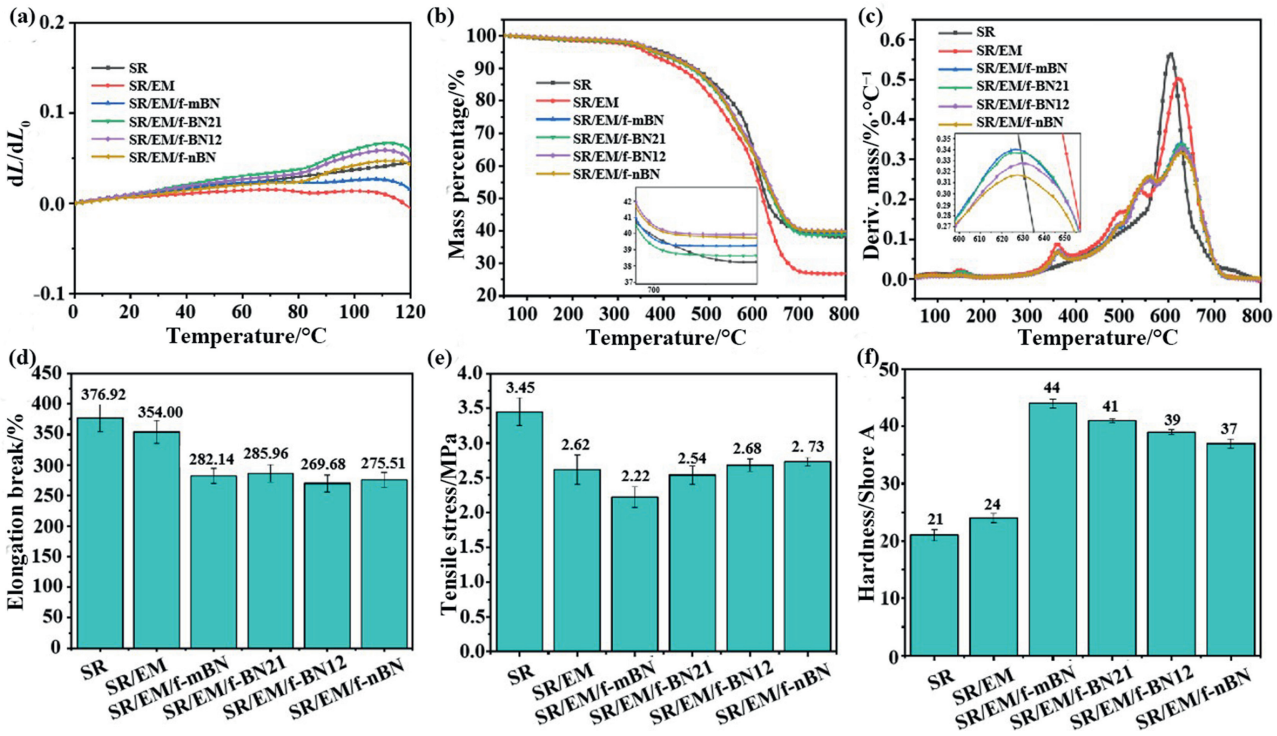

Fig. 3. (a) Thermal expansion curves; (b) TGA and (c) DTG curves; (d) elongation at break and (e) tensile strength; (f) Shore hardness of SR and its composite foams.

polymer is also increased, and the probability of bonding between the particles to form a thermal conduction path is lower.

Fig. 3(a) shows the thermal expansion curves of SR and its composite foams in the temperature range of 0–120 °C. The figure shows that the dimensional change of pure SR in the tested temperature range shows a good linear relationship with temperature, with a dimensional change of 4.50% at 120 °C. Comparison of the four samples with the addition of f-BN reveals that the SR/EM/f-nBN composites with the addition of nano-sized boron nitride have the smallest volume expansion and contraction, and the final dimensional change is closest to that of pure SR, which may be attributed to the fact that the smaller the size of f-BN, the more interfaces are formed with the matrix, and the stronger the interaction force is, which is capable of better restricting the thermal movement of the polymer chain segments and thus controlling the volume contraction and expansion process of the composites. Fig. 3(b) and (c) show the TGA and derivative thermogravimetry (DTG) curves of SR and its composite foams under a nitrogen atmosphere. It can be found that pure SR gradually starts to degrade at about 300 °C and reaches the maximum rate of mass loss at about 600 °C until the mass is basically stabilized at about 700 °C, a process that mainly corresponds to the breakage of the side groups of the silicone rubber and the degradation of the main chain. It was found that the maximum mass loss rate of the samples with f-BN was in the order of "SR/EM/f-mBN > SR/EM/f-BN21 > SR/EM/f-BN12 > SR/EM/f-nBN", which could be attributed to the fact that the smaller the size of f-BN, the larger the interfacial bonding area and the stronger the interaction force with the matrix. The larger the size of f-BN, the stronger the interaction force and the stronger the restriction on the thermal movement of silicone rubber molecular chains. The amount of residual char of pure SR at 800 °C is 38.3% (mass), and the amount of residual char of the samples of SR/EM is only 26.9% (mass). After adding f-BN, the residual char of the composite foams increased to 38.6%–40.0% (mass), which was higher than that of pure SR, thanks to the high thermal stability of BN itself and the strong interaction between f-BN and the SR matrix.

3.3. Mechanical properties of SR/EM/f-BN composite foams

The mechanical properties of SR and its composite foams were investigated by tensile testing and hardness testing. Fig. 3(d) and (e) show the elongation at break and tensile strength of SR and its composite foams after tensile testing. The elongation at break of pure SR was higher at 376.92%, and that of the foam with the addition of EM was reduced to 354.00%. After the addition of f-BN with different particle sizes, the elongation at break of each composite foam was further reduced to vary from 269.68% to 285.96%, which may be due to the fact that a larger number of portions of f-BN were added in this section, which created some defects inside the material, and so the elongation at break decreased instead. As shown in Fig. 3(e), the tensile strength of pure SR was 3.45 MPa, that of the SR/EM/f-mBN with the addition of f-mBN was 2.22 MPa, while the tensile strength of SR/EM/f-nBN with the addition of f-nBN has a tensile strength of 2.73 MPa. The tensile strength of the composite foams increases with the decrease in the particle size of the f-nBN, which is due to the fact that the smaller the particle size

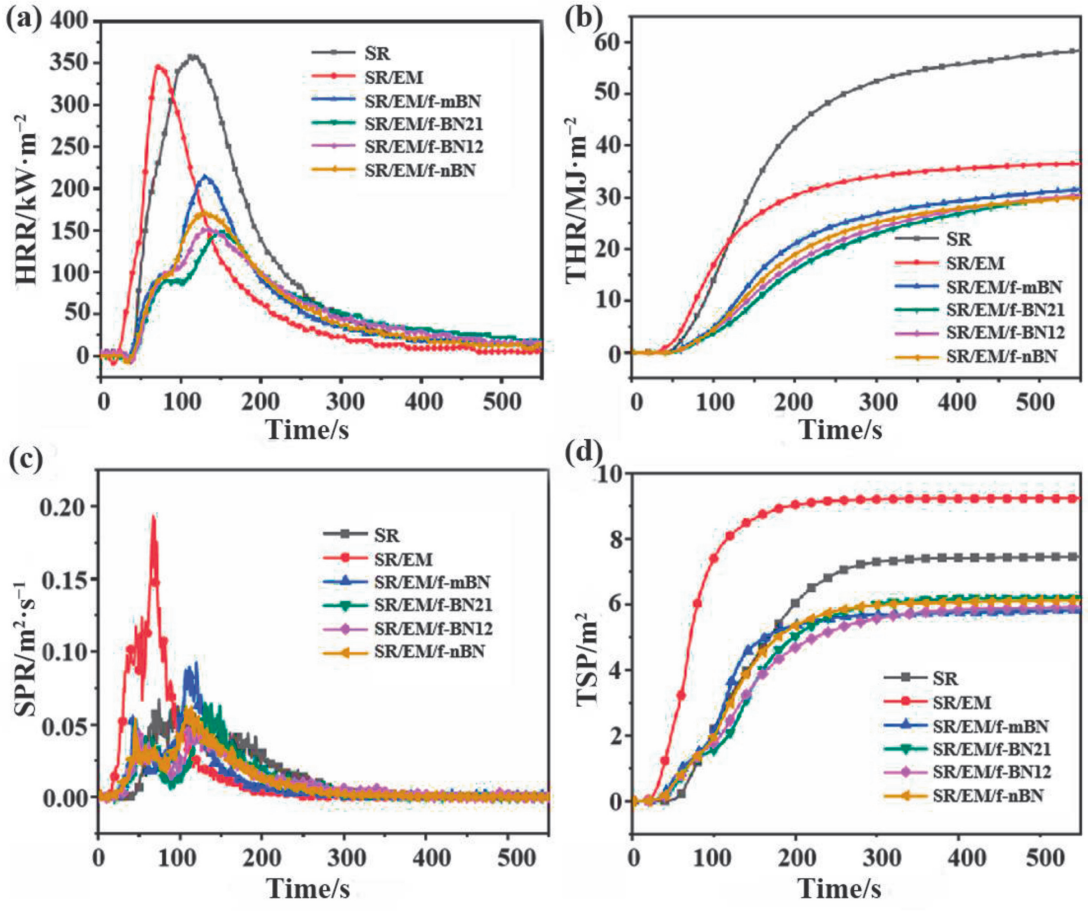

Fig. 4. (a) HRR; (b) THR; (c) SPR and (d) TSP curves of SR and its composite foams.

is, the larger is the interfacial area between BN and the matrix, and the stronger is the interaction. Fig. 3(f) shows the hardness test results of SR and its composite foams. Pure SR has better elasticity, and the hardness is only 21 HA. After continuing to add f-BN with different particle sizes, the hardness of the composite foams further increased from 37 to 44 HA, which is due to the fact that BN is a rigid material with high hardness. The hardness of the samples with f-BN added is ranked as "SR/EM/f-mBN > SR/EM/f-BN21 > SR/EM/f-BN12 > SR/EM/f-nBN", which may be due to the fact that f-mBN has a larger size and thickness and is relatively rigid and less prone to deformation. The composite foam with added micron-sized BN is stiffer.

3.4. Flame retardancy of SR/EM/f-BN composite foams

The fire safety of SR and its composite foams was investigated by cone experiments. Fig. 4(a) and (b) show the heat release rate (HRR) and total heat release (THR) curves of SR and its composite foams, and the detailed data are shown in Table 2. Thanks to the high thermal stability and physical barrier effect of f-BN, the composite foams with different particle sizes of f-BN have significantly lower values of Peak of heat release rate (PHRR) and THR, and the t_{PHRR} also increases significantly. Comparatively, the PHRR values of the samples with f-BN were ranked as "SR/EM/f-mBN > SR/EM/f-nBN > SR/EM/f-BN12 > SR/EM/f-BN21", which shows that f-nBN has a better effect on the reduction of HRR than the f-mBN, and because the f-nBN will fill into the voids of the f-mBN during the material molding process, a denser physical barrier, a better blocking effect. The fire growth index (FGI), which is the ratio of the PHRR of material to the time taken to reach the peak, can be used to measure the fire spreading performance of material, and the detailed data are given in Table 2. The change rule of FGI value of the composite foam with added f-BN was consistent with PHRR, and the fire hazard was significantly reduced, in which the SR/EM/f-BN21 sample had the lowest FGI value of 0.97 $kW \cdot s^{-1} \cdot m^{-2}$, which was 31.9% of that of pure SR. The amount of residual char after combustion of pure SR was 57.3% (mass), and the residual char mass of the foam with only EM added was reduced to 41.1% (mass), whereas the char formation of the samples with f-BN added was significantly higher, and more residual char could effectively insulate the heat and retard the exchange of oxygen and gas phase products between the matrix and the combustion region. Fig. 4(c) and (d) show the smoke production rate (SPR) and total smoke production (TSP) curves of SR and its composite foams. The peak SPR of pure SR was 0.05 $m^2 \cdot s^{-1}$, and the TSP value was 7.45 m^2. Because EM is composed of carbon-based polymer on the outside and low-boiling paraffin on the inside, more flue gas is produced during incomplete combustion, so the SPR peak value of SR/EM foam is increased to about 0.20 $m^2 \cdot s^{-1}$, and the TSP value is increased to 9.22 m^2. After adding f-BN, the SPR value of the composite foam is significantly lower than that of SR/EM, which is similar to that of pure SR, and the TSP value is significantly lower than that of pure SR, and the smoke hazard is significantly reduced, and fire safety is improved.

The char residue of the sample was further analyzed by SEM. Fig. 5 shows the SEM images of the internal char residue of SR, SR/

Table 2
Cone results of SR and its composite foams

Sample	PHRR/$kW \cdot m^{-2}$	THR/$MJ \cdot m^{-2}$	t_{PHRR}/s	FGI/$kW \cdot s^{-1} \cdot m^{-2}$	Residue char/% (mass)
SR	356.2	58.4	117	3.04	57.3
SR/EM	346.7	36.5	73	4.75	41.1
SR/EM/f-mBN	213.8	31.5	131	1.63	60.4
SR/EM/f-BN21	148.1	30.4	152	0.97	63.6
SR/EM/f-BN12	151.6	30.5	134	1.13	62.8
SR/EM/f-nBN	171.8	30.0	132	1.30	64.0

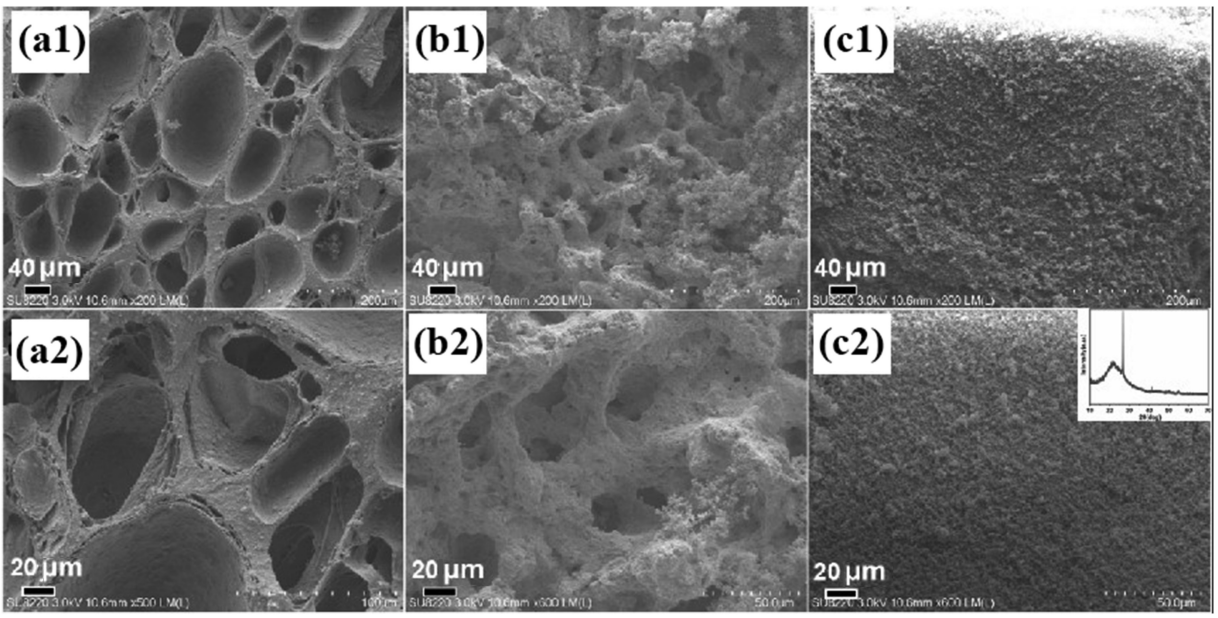

Fig. 5. SEM images of char residues in (a) SR, (b) SR/EM and (c) SR/EM/f-BN21 composite foams; the illustration shows the corresponding XRD pattern.

EM, and SR/EM/f-BN21 composite foams. It can be seen that the inner layer of the residual char of pure SR has many pores tens to hundreds of microns in size, some of which are direct to the matrix. The internal char residue of the SR/EM foam material with EM added is still a bubble-like structure with many pores, but some flocculent substances are attached to the carbon-silicon skeleton, which may be the residue after the combustion of the EM shell. The internal char residue of SR/EM/f-BN21 has undergone significant changes; the originally large pores have been blocked, and the char layer has become very dense and compact. In addition to a wide diffraction peak, the XRD pattern in the figure also shows a characteristic peak that can be attributed to BN. It can be inferred that the BN layer remaining in the carbon slag constitutes a dense physical barrier, inhibiting the combustion process of the SR matrix [22–24].

4. Conclusions

On the basis of EM foaming, modified BN with different particle sizes is added to the SR composite foams. The results show that the thermal conductivity, electrical insulation, thermal stability, and flame retardant properties of the composite foams are significantly improved after adding f-BN, and D_k and D_f are still much lower than pure SR. It is found that when the ratio of f-mBN and f-nBN is 2:1, the thermal conductivity of the composite reaches the maximum value of 0.808 $W \cdot m^{-1} \cdot K^{-1}$, which is caused by the improvement of the packing tightness of f-BN in the foam. Moreover, f-nBN improved the electrical insulation and tensile strength of materials better than f-mBN, but f-mBN improved the dielectric properties and thermal conductivity of materials better than f-nBN. The flame retardancy mechanism was explored through condensed phase analysis, and the char layer quality of the composite foams with f-BN added was better. The improved flame retardancy is mainly attributed to the high thermal stability and physical barrier effect of f-BN.

Declaration of Interest

We declare that we have no financial and personal relationships with other people or organizations that can inappropriately influence our work.

Acknowledgements

The work was financially supported by the Natural Science Foundation of Anhui Province (2108085QE211), National Natural Science Foundation of China (22205229) and Science Foundation of China University of Petroleum, Beijing (2462024QNXZ001).

Supplementary Material

Supplementary data to this article can be found online at https://doi.org/10.1016/j.cjche.2024.01.012.

References

[1] B.L. Wang, G.Y. Li, L. Xu, J.H. Liao, X.T. Zhang, Nanoporous boron nitride aerogel film and its smart composite with phase change materials, *ACS Nano* 14 (12) (2020) 16590–16599.
[2] X.F. Wu, B. Tang, J. Chen, L.M. Shan, Y. Gao, K. Yang, Y. Wang, K. Sun, R.H. Fan, J. H. Yu, Epoxy composites with high cross-plane thermal conductivity by constructing all-carbon multidimensional carbon fiber/graphite networks, *Compos. Sci. Technol.* 203 (2021) 108610.
[3] X.D. Zhang, Y. Guo, Y.J. Liu, Z. Li, W.Z. Fang, L. Peng, J. Zhou, Z. Xu, C. Gao, Ultrathick and highly thermally conductive graphene films by self-fusion, *Carbon* 167 (2020) 249–255.
[4] M. Wu, Y.L. Zhou, H. Zhang, W.G. Liao, 2D boron nitride nanosheets for smart thermal management and advanced dielectrics, *Adv. Mater. Interfaces* 9 (25) (2022) 2200610.
[5] Y.C. Liu, Z. Hu, H.H. Wu, S. Sun, L.H. Chen, K. Wu, X.L. Lin, Y.L. Qin, *In-situ* construction of dense thermal conduction networks endow the polymeric composites with advanced thermal management capability and superior dielectric properties, *Chem. Eng. J.* 449 (2022) 137753.
[6] S.Q. Yang, W.Z. Li, S.B. Bai, Q. Wang, Fabrication of morphologically controlled composites with high thermal conductivity and dielectric performance from aluminum nanoflake and recycled plastic package, *ACS Appl. Mater. Interfaces* 11 (3) (2019) 3388–3399.
[7] X.Y. Yu, M.R. Bhatti, X.T. Ren, P. Steiner, F. Di Sacco, M. Dong, H. Zhang, D. Papageorgiou, G. Portale, C. Kocabas, C.W.M. Bastiaansen, M. Reece, H.X. Yan, E. Bilotti, Dielectric polymer composites with ultra-high thermal conductivity and low dielectric loss, *Compos. Sci. Technol.* 229 (2022) 109695.
[8] X.R. Liu, W. Wu, C. Liu, Y. Wang, Q.M. Chen, S.F. Cui, Preparation and mechanism research of bio-inspired dopamine decorated expanded graphite/silicone rubber composite with high thermal conductivity and excellent insulation, *Nanotechnology* 32 (32) (2021) 325702.
[9] J.J. Zheng, S.J. He, J.Q. Wang, W.X. Fang, Y. Xue, L.M. Xie, J. Lin, Performance of silicone rubber composites filled with aluminum nitride and alumina tri-hydrate, *Materials* 13 (11) (2020) 2489.
[10] Z.Q. Zou, W. Wu, Y. Wang, L. Wang, Enhancement of thermal conductivity and tensile strength of liquid silicone rubber by three-dimensional alumina network, *Soft Mater.* 17 (3) (2019) 297–307.
[11] S.S. Dai, Y. Liu, Z.Y. Huang, X.W. Zhao, Molecular dynamics simulations on the interaction between microsphere and water in nanosilica/crosslinked polyacrylamide microsphere aqueous solution with a core–shell structure and its swelling behavior, *Compos. Interfaces* 25 (1) (2018) 69–92.
[12] J. Loomis, P. Xu, B. Panchapakesan, Stimuli-responsive transformation in carbon nanotube/expanding microsphere-polymer composites, *Nanotechnology* 24 (18) (2013) 185703.
[13] H. Luo, X.D. Wang, Y.D. Wen, S.D. Li, T.Y. Zhang, C.D. Jiang, F.F. Wang, L.Q. Liu, H.B. Yu, Self-sensing scanning superlens for three-dimensional noninvasive visible-light nanoscale imaging on complex surfaces, *Nano Lett.* 23 (10) (2023) 4311–4317.
[14] M. Xiang, R.M. Yang, J.J. Yang, S.L. Zhou, J. Zhou, S. Dong, Fabrication of polyamide 6/reduced graphene oxide nano-composites by conductive cellulose skeleton structure and its conductive behavior, *Compos. Part B Eng.* 167 (2019) 533–543.
[15] X. Xie, D. Yang, Construction of thermal conduction networks and decrease of interfacial thermal resistance for improving thermal conductivity of epoxy natural rubber composites, *Ceram. Int.* 49 (11) (2023) 17650–17659.
[16] L. Zhang, Z.F. Li, G.T. Liu, R. Chen, S.Y. Guo, Enhancement of the electrical and thermal conductivity of epoxy-based composite films through the construction of the multi-scale conductive bridge structure, *Compos. Sci. Technol.* 239 (2023) 110074.
[17] S. Chen, W.K. Xing, H. Wang, W.Z. Cheng, Z.H. Lei, F.Y. Zheng, P. Tao, W. Shang, B.W. Fu, C.Y. Song, M.D. Dickey, T. Deng, A bottom-up approach to generate isotropic liquid metal network in polymer-enabled 3D thermal management, *Chem. Eng. J.* 439 (2022) 135674.
[18] G.Z. Tang, L. Wang, D.G. Li, Predetermined thermal conductivity porous medium generated by conditional generation adversarial network, *Acta Phys. Sin.* 70 (5) (2021) 054401.
[19] S. Graham, S. Choi, Integrating boron arsenide into power devices, *Nat. Electron.* 4 (6) (2021) 380–381.
[20] S.S. Li, S.H. Qi, N.L. Liu, P. Cao, Study on thermal conductive BN/novolac resin composites, *Thermochim. Acta* 523 (1–2) (2011) 111–115.
[21] C.Y. Wang, B. Wu, X. Mao, T. Deng, R. Li, Y. Xu, X.Z. Tang, The effects of concentration and particle size of TiO_2 on the dielectric properties of polyolefin-based microwave substrates, *ChemistrySelect* 5 (4) (2020) 1464–1469.
[22] Y.B. Huang, S.H. Jiang, R.C. Liang, P. Sun, Y. Hai, L. Zhang, Thermal-triggered insulating fireproof layers: a novel fire-extinguishing MXene composites coating, *Chem. Eng. J.* 391 (2020) 123621.
[23] P. Sun, N. Cai, X. Zhong, X. Zhao, L. Zhang, S. Jiang, Facile monitoring for human motion on fireground by using MiEs-TENG sensor, *Nano Energy* 89 (2021) 106492.
[24] L. Zhang, Y.B. Huang, H.R. Dong, R.Z. Xu, S.H. Jiang, Flame-retardant shape memory polyurethane/MXene paper and the application for early fire alarm sensor, *Compos. Part B Eng.* 223 (2021) 109149.